Deblurring of Color Images Corrupted by Impulsive Noise

Leah Bar, Alexander Brook, Nir Sochen and Nahum Kiryati, *Senior Member, IEEE*

Abstract

We consider the problem of restoring a multichannel image corrupted by blur and impulsive noise (e.g. salt-and-pepper noise). Using the variational framework, we consider the L^1 fidelity term and several possible regularizers. In particular, we use generalizations of the Mumford-Shah functional to color images and Γ-convergence approximations to unify deblurring and denoising. Experimental comparisons show that the Mumford-Shah stabilizer yields better results with respect to Beltrami and Total Variation regularizers. Color edge detection is a beneficial by-product of our methods.

Index Terms

Mumford-Shah functional, impulse noise, deblurring, denoising, color image processing.

I. Introduction

In this work we consider the problem of restoring a color image degraded by blur and high impulsive noise level. Deblurring and denoising are probably two of the most studied problems in image processing. But while most of the literature on deblurring and denoising either considers these problems separately, or deals with deblurring at very low noise level, in the specific problem we deal with here, both tasks are performed simultaneously.

The deconvolution problem (also referred to as deblurring or more generally as restoration) has a long and rich history, which can be traced by an interested reader with the help of reviews by Demoment [1], Biemond *et al.* [2], Banham and Katsaggelos [3], and Puetter *et al.* [4]. The overwhelming majority of the works on deblurring consider the case of blurred *gray-level* images with a small amount of additive Gaussian noise [5], [6], [7], [8], [9], [10]. A promising and efficient method to solve this problem even in the presence of high noise level was proposed by Neelamani *et al.* [11], where hybrid Fourier-wavelet regularization was used in the deconvolution process. Nikolova *et al.* [12] incorporated the piecewise Gaussian Markov random field model in the regularization term. This formulation can be viewed as half-quadratic regularization [9], [10], which leads to a truncated quadratic function of the image gradients. Image recovery with non-differentiable regularization

L. Bar is with the Department of Electrical and Computer Engineering, University of Minnesota.

A. Brook is with the Dept. of Mathematics, Technion, Israel.

N. Sochen is with the Dept. of Applied Mathematics, Tel-Aviv University, Israel.

N. Kiryati is with the School of Electrical Engineering, Tel-Aviv University, Israel.

terms was analyzed and implemented by Combettes and Luo [13]. Nikolova [12] investigated the cost functional characteristics in terms of weakly constrained minimization. The relation between smooth and non-smooth regularizers was analyzed and illustrated by image restoration experiments. A significant contribution for the solution of inverse problem via a non-smooth fidelity term was given by Nikolova [14], [15]. This idea was exploited to gray-level image denoising corrupted by salt-and-pepper noise [16]. In the present study we expand this concept for color image deblurring and impulsive noise removal.

Color image restoration has been mostly investigated in three main branches: image denoising in the presence of Gaussian noise, image deconvolution in the presence of Gaussian noise, and impulse noise removal. For detailed reviews see Galatsanos *et al.* [17], Brook *et al.* [18] and Tschumperlé [19].

There are many *image denoising* methods that are specific to color images. Some of the more relevant to the present work are those of Di Zenzo [20], Cumani [21], Sapiro and Ringach [22], Blomgren [23] and Sochen, Kimmel and Malladi [24]. These papers propose smoothness measures for multichannel images that can be used in a variational framework. However, they either do not specify the noise model, or assume that the noise is Gaussian.

Barash [25] and later Welk *et al.* [26] proposed a variational scheme based on the Perona-Malik [27] smoothness term to the multichannel *deconvolution* problem. Barash treats each channel separately, while Welk *et al.* introduce channel coupling. Both works treat images with low Gaussian noise levels. The work of Molina *et al.* [28] is based on Bayesian Maximum a Posteriori methods and a fully discrete formulation that uses a separate line process for each channel. A cross term is introduced to provide coupling between the line processes of different channels. This formulation can be seen, in a way, as a discretization of the Mumford-Shah functional. In this sense, it is similar to one of the methods we present here.

Methods for *removal of impulse noise* from color images include vector median filter [29], vector directional filter [30], [31] and methods that combine noise detection with noise removal [32], [33] (see also the review [34]). Each of these studies has several variants and combinations, see e.g. the review in [16].

In this paper we concentrate on variational methods which recover multichannel images that underwent significant blur and are contaminated by high-density (30% and more) impulsive noise (salt-and-pepper or random valued noise). Image restoration and noise removal are concurrently performed in a unified framework. The advantage of simultaneous deconvolution and denoising over a sequential process (where denoising precedes deconvolution) is exemplified by the authors in [35]. In addition, we have shown in [36] that the Mumford-Shah regularizer in its Γ-convergence approximation is an extended version of the Geman-McClure potential function. Here we generalize our preliminary work [35] to the multichannel case.

The rest of the paper is organized as follows. Section II presents several variational formulations of the deconvolution and impulse noise removal tasks. Section III provides the numerical details of the minimization procedure. A robust statistics interpretation of some of the presented cost-functionals is given in section IV, and experimental results are shown in section V. The conclusions are in section VI.

II. PROPOSED FUNCTIONALS

A. Variational Framework

Let Ω denote an open bounded set in $\mathbb{R}^2$ on which the image intensity function $u : \Omega \rightarrow [0, 1]$ is defined. The gradient of the image is given by $\nabla u = (\partial u/\partial x, \partial u/\partial y)^T$ and dA stands for area element. The standard model for blurred and noisy images is given by $z = h * u + n$ where u is the ideal underlying image, z is the observed image, h is linear and space-invariant blur kernel, n is additive Gaussian noise independent on u and $*$ stands for the convolution operator. Our approach to the image restoration problem is within the variational framework. Specifically, we consider minimization problems of the form

$$\mathcal{F}(u) = \min_u \big(\mathcal{I}(h * u - z) + \mathcal{J}(\nabla u)\big). \tag{1}$$

The fidelity term $\mathcal{I}(h * u - z)$ forces the smoothed image $h * u$ to be close to the observed image z. The smoothness term $\mathcal{J}(\nabla u)$ enforces a smoothness constraint on u, and can be seen as a regularizer in the ill-posed deconvolution problem. Adopting the robust statistics notations of Huber [37] and Black and Rangarajan [38], the error norm $\mathcal{I}$ will be expressed in terms of a robust ρ-function. In this context the robust function is not necessarily convex. The contribution of this work relies on the integration of L^1-based fidelity terms that are better suited for dealing with impulsive noise [14], [15] and Mumford-Shah based regularizers to solve the *color* deconvolution problem together with color impulse noise removal. These combinations will be proved to be successful from both theoretical and experimental viewpoints.

B. Fidelity Term

The commonly used model of white Gaussian noise $n \sim N(0, \sigma^2)$ leads by the maximum likelihood estimation to the minimization of the L^2 norm of the noise,

$$\min_u ||h * u - z||^2_{L^2}. \tag{2}$$

However, practical systems suffer from *outliers* where few or more pixels do not obey the Gaussian noise model and can be much noisier than others. Salt-and-pepper noise for instance, is considered as an outlier and may be due to various causes, such as bit errors in transmission or malfunctioning camera pixels. Minimization of outlier effects can be accomplished by replacing the quadratic form (2) with a robust ρ-function [37].

In the case of multichannel images, the image intensity is defined as $u : \Omega \rightarrow [0, 1]^3$. Here z^σ denotes the observed image at channel $\sigma \in \{r, g, b\}$ such that $z^\sigma = h * u^\sigma + n^\sigma$. Multichannel outliers can be formed in several ways. The first case we present - Independent Channels Independent Location (ICIL), occurs whenever the damaged pixels are randomly located in the image at random channels, i.e. the noise $n^\sigma(x, y)$ is an independent random variables in both location and channel. This means that a damaged pixel $z^{\sigma_1}(x_1, y_1)$ is independent on another damaged pixel $z^{\sigma_2}(x_2, y_2)$. Eq. (3) is the negative log-likelihood representation of such case where the logarithms of the noise probabilities are summed.

$$\mathcal{I} = \int_\Omega \sum_\sigma \rho(h * u^\sigma - z^\sigma)\, dA, \tag{3}$$

where $\sigma \in \{r, g, b\}$. In the second case - Dependent Channels Independent Location (DCIL),

$$\mathcal{I} = \int_\Omega \rho \left(\sum_\sigma (h * u^\sigma - z^\sigma) \right) dA, \tag{4}$$

the location (x, y) of a damaged pixel is independent on the location of any other damaged pixel (x_1, y_1). However, there might be some channel-dependence. This means that a damaged pixel $z^{\sigma_1}(x, y)$, might be corrupted at the same location in another channel $z^{\sigma_2}(x, y)$ as well. Thus, the summation (integration) is only over the pixels. As for the third possible case - Independent Channels Dependent Location (ICDL), if some pixel $z^{\sigma_1}(x, y)$ is damaged, the pixels in its vicinity at the same channel σ_1 might be damaged as well. In the current study this case will not be considered.

C. Smoothness Term

In this section we present several possibilities for the smoothness term. The first smoothness term we present is a channel-by-channel extension of the Total Variation regularizer [5]

$$\mathcal{J}(u) = \beta \sum_\sigma \int_\Omega |\nabla u^\sigma| \, dA.$$

Since the channels are separately processed, spurious color artifacts can be formed because the locations of edges do not necessarily overlap in the different channels. Examples of such artifacts can be found in [18], [28]. The channel coupling can be formulated in several forms. Blomgren and Chan [39] for example, presented color TV regularization.

$$\sqrt{\left[\int |\nabla u^r|\right]^2 + \left[\int |\nabla u^g|\right]^2 + \left[\int |\nabla u^b|\right]^2}.$$

A different generalization of Total Variation regularization to color images with *coupled* channels takes the form [18]

$$\begin{aligned} \mathcal{J}^{TV}(u) &= \beta \int_\Omega ||\nabla u|| \, dA \\ &= \beta \int_\Omega \sqrt{|\nabla u^r|^2 + |\nabla u^g|^2 + |\nabla u^b|^2} \, dA. \end{aligned} \tag{5}$$

In the present study we used the latter term. Both expressions yield similar experimental results.

An alternative approach is the Beltrami flow introduced by Sochen *et al.* [24]. Its superiority with respect to Color TV regularization has been shown by Tschumperlé [19]. In the Beltrami framework, a color image (u^r, u^g, u^b) is regarded as a two-dimensional surface embedded in $\mathbb{R}^5$-space spanned by (x, y, u^r, u^g, u^b). The area of this surface is given by

$$\int_\Omega \sqrt{\det G} \, dA,$$

where the metric tensor G induced on the surface is given by

$$G = \begin{pmatrix} 1 + \gamma^2 \sum_\sigma (u_x^\sigma)^2 & \gamma^2 \sum_\sigma u_x^\sigma u_y^\sigma \\ \gamma^2 \sum_\sigma u_x^\sigma u_y^\sigma & 1 + \gamma^2 \sum_\sigma (u_y^\sigma)^2 \end{pmatrix}.$$

Here γ is a coefficient that describes the relative scales of the space coordinates x, y on one hand and the color coordinates u^r, u^g, u^b on the other hand.

This surface area is a measure of image smoothness, and since we assume that each color is equally important this measure has the important advantage of color channels alignment. This becomes more obvious if we rewrite it as

$$\int_\Omega \sqrt{\det G}\; dA = \int_\Omega \sqrt{1+\gamma^2 \sum_\sigma (|\nabla u^\sigma|^2) + \frac{\gamma^4}{2} \sum_{\sigma_1,\sigma_2} |\nabla u^{\sigma_1} \times \nabla u^{\sigma_2}|^2} dA,$$

where $\times$ denotes the cross-product of ∇u^{σ_1} and ∇u^{σ_2}. Minimizing the cross-product between the gradient vectors enforces the color channels u^σ, $\sigma \in \{r, g, b\}$ to be aligned together as they get smoother in scale [40]. The Beltrami regularizer is thus defined as

$$\mathcal{J}^{BEL} = \beta \int_\Omega \sqrt{\det(G)}\; dA. \tag{6}$$

Reflecting the preference for piecewise smooth images, two terms of the Mumford-Shah (MS) segmentation functional [41] can be used for regularization in image restoration [42]. In this stabilizer, the energy assigned to a gray level image depends not only on the image $u : \Omega \to [0, 1]$ itself, but also on the set of edges $K \subset \Omega$ and is given by

$$\mathcal{J}^{MS}(u, K) = \beta \int_{\Omega \setminus K} |\nabla u|^2 dA + \alpha \int_K d\mathcal{H}^1.$$

The first term enforces the smoothness of u everywhere except in the discontinuity set K. The second term minimizes the one-dimensional Hausdorff measure (length) of the discontinuity set. Using the Γ-convergence framework, Ambrosio and Tortorelli [43] approximated this functional by a sequence of local functionals

$$\begin{aligned} \mathcal{J}_\varepsilon^{MS}(u, v) =& \beta \int_\Omega v^2 |\nabla u|^2\; dA \\ &+ \alpha \int_\Omega \left(\varepsilon |\nabla v|^2 + \frac{(v-1)^2}{4\varepsilon} \right)\; dA. \end{aligned} \tag{7}$$

The auxiliary function $v(x)$ represents the edges—it is close to 1 in the smooth parts of the image and close to 0 near the edges. The minimizers of $\mathcal{J}_\varepsilon^{MS}$ approach the minimizers of $\mathcal{J}^{MS}$ as $\varepsilon \to 0$.

In the color version of this functional, suggested by Brook *et al.* [18], the magnitude of the gradient $|\nabla u|$ is replaced by the Frobenius norm of the matrix ∇u:

$$||\nabla u|| = \sqrt{\sum_\sigma \left[(u_x^\sigma)^2 + (u_y^\sigma)^2 \right]}\; . \tag{8}$$

Note that in the $\mathcal{J}_\varepsilon^{MS}$ regularizer (Eq. 7) the edge map v is common for the three channels and provides the necessary coupling between colors.

A modified version of this approximation to the Mumford-Shah functional for gray-level images was suggested by Shah [44]:

$$\begin{aligned} \mathcal{J}_\varepsilon^{MSTV}(u, v) =& \beta \int_\Omega v^2 |\nabla u|\; dA \\ &+ \alpha \int_\Omega \left(\varepsilon |\nabla v|^2 + \frac{(v-1)^2}{4\varepsilon} \right)\; dA. \end{aligned} \tag{9}$$

In this version the L^2 norm of ∇u was replaced by the L^1 norm in the first term. Alicandro *et al.* [45] proved the Γ-convergence of this functional to

$$\begin{aligned}\mathcal{J}^{MSTV} =&\beta \int_{\Omega\setminus K} |\nabla u|\ dA \\ &+\alpha \int_K \frac{|u^+ - u^-|}{1+|u^+ - u^-|} d\mathcal{H}^1 + |D^c u|(\Omega),\end{aligned}$$

where u^+ and u^- denote the image values on two sides of the edge set K, $\mathcal{H}^1$ is the one-dimensional Hausdorff measure and $D^c u$ is the Cantor part of the measure-valued derivative Du. This functional was generalized by Brook *et al.* [18] for color images where the Frobenius norm (8) was used in this case as well.

The last smoothness term we present is the generalization of the MS regularizer together with the geometric model of the Beltrami flow suggested by Brook *et al.* [18] such that

$$\begin{aligned}&\mathcal{J}^{MSBEL}(u,K) = \\ &\beta \int_{\Omega\setminus K} \left(||\nabla u||^2 + \gamma \sum_{\sigma 1,\sigma 2} |\nabla u^{\sigma_1} \times \nabla u^{\sigma_2}| \right)\ dA + \alpha \int_K d\mathcal{H}^1.\end{aligned}$$

where the approximated sequence is given by

$$\begin{aligned}\mathcal{J}_\varepsilon^{MSBEL}(u,v) =&\beta \int_\Omega v^2 \left(||\nabla u||^2 + \gamma |u_x \times u_y| \right)\ dA \\ &+\alpha \int_\Omega \left(\varepsilon |\nabla v|^2 + \frac{(v-1)^2}{4\varepsilon} \right)\ dA.\end{aligned} \tag{10}$$

More details about the Γ-convergence proof of (10) can be found in [18].

III. Numerical methods

Minimization of the cost functionals is carried out using the Euler-Lagrange equations with homogeneous Neumann boundary conditions $\partial u^\sigma/\partial N = 0$, $\partial v/\partial N = 0$, where N is the normal to the image boundary. We present the Euler-Lagrange equations of the five regularizers that we consider. The following functionals consist of the structure of Eq. (1) with the corresponding regularizers. The fidelity $\mathcal{I}$ takes the form of Eq. (3) using the modified L^1 norm:

$$\mathcal{I} = \int_\Omega \sum_\sigma \sqrt{(h * u^\sigma - z^\sigma)^2 + \eta}\, dA \tag{11}$$

with $0 < \eta \ll 1$ to gain numerical stability.

For the Total Variation regularization (5), the Euler-Lagrange equation is

$$\begin{aligned}\frac{\delta \mathcal{F}^{TV}}{\delta u^\sigma} =&\frac{h * u^\sigma - z^\sigma}{\sqrt{(h * u^\sigma - z^\sigma)^2 + \eta}} * h(-x,-y) \\ &-2\beta\ \nabla \cdot \left(\frac{\nabla u^\sigma}{||\nabla u||} \right) = 0.\end{aligned} \tag{12}$$

The Beltrami Euler-Lagrange equation takes the form

$$\begin{aligned}\frac{\delta \mathcal{F}^{BEL}}{\delta u^\sigma} =&\frac{h * u^\sigma - z^\sigma}{\sqrt{(h * u^\sigma - z^\sigma)^2 + \eta}} * h(-x,-y) \\ &-\beta \nabla \cdot \left(\sqrt{\det(G)}\ G^{-1}\ \nabla u^\sigma \right) = 0.\end{aligned} \tag{13}$$

The parameter β can be made adaptive [46]. However, here β is replaced by $\beta/\sqrt{\det(G)}$ in order to convert the regularizer to a geometric operator known as Laplace-Beltrami [47].

The objective functionals with the smoothness term based on the variants of the Mumford-Shah functional (7), (9) depend on the recovered image u and on the edge map v. With MS regularization (7), the Euler-Lagrange equations are

$$\begin{aligned}\frac{\delta \mathcal{F}_{\varepsilon}^{MS}}{\delta u^{\sigma}} =& \frac{h * u^{\sigma} - z^{\sigma}}{\sqrt{(h * u^{\sigma} - z^{\sigma})^2 + \eta}} * h(-x,-y) \\ & -2\beta \nabla \cdot (v^2 \nabla u^{\sigma}) = 0,\end{aligned} \tag{14}$$

$$\frac{\delta \mathcal{F}_{\varepsilon}^{MS}}{\delta v} = 2\beta v ||\nabla u||^2 + \alpha \left(\frac{v-1}{2\varepsilon} \right) - 2\varepsilon\ \alpha \nabla^2 v = 0. \tag{15}$$

For MSTV regularization (9), the L^1 norm $||\nabla u||$ is replaced by the modified L^1 norm $\sqrt{||\nabla u||^2 + \mu}$. Thus,

$$\begin{aligned}\frac{\delta \mathcal{F}_{\varepsilon}^{MSTV}}{\delta u^{\sigma}} =& \frac{h * u^{\sigma} - z^{\sigma}}{\sqrt{(h * u^{\sigma} - z^{\sigma})^2 + \eta}} * h(-x,-y) \\ & -2\beta \nabla \cdot \left(\frac{v^2 \nabla u^{\sigma}}{\sqrt{||\nabla u||^2 + \mu}} \right) = 0,\end{aligned} \tag{16}$$

and

$$\frac{\delta \mathcal{F}_{\varepsilon}^{MSTV}}{\delta v} = 2\beta v \sqrt{||\nabla u||^2 + \mu} + \alpha \left(\frac{v-1}{2\varepsilon} \right) - 2\varepsilon\ \alpha \nabla^2 v = 0. \tag{17}$$

Finally, for the MSBEL regularization (10) the Euler-Lagrange equations are

$$\begin{aligned}&\frac{\delta \mathcal{F}_{\varepsilon}^{MSBEL}}{\delta u^{\sigma}} = \frac{h * u^{\sigma} - z^{\sigma}}{\sqrt{(h * u^{\sigma} - z^{\sigma})^2 + \eta}} * h(-x,-y) - \beta \nabla \cdot \\ &\left[v^2 \left(2u_x^{\sigma} + \gamma \frac{[u_y \times (u_x \times u_y)]^{\sigma}}{|u_x \times u_y|}, 2u_y^{\sigma} - \gamma \frac{[u_x \times (u_x \times u_y)]^{\sigma}}{|u_x \times u_y|} \right) \right] \\ &= 0,\end{aligned} \tag{18}$$

and

$$\begin{aligned}\frac{\delta \mathcal{F}_{\varepsilon}^{MSBEL}}{\delta v} =& 2\beta v \left(||\nabla u||^2 + \gamma |u_x \times u_y| \right) \\ & + \alpha \left(\frac{v-1}{2\varepsilon} \right) - 2\varepsilon\ \alpha \nabla^2 v = 0.\end{aligned} \tag{19}$$

It can be easily seen that Eqs. (12,13,14,16,18) are nonlinear integro-differential equations. Following Vogel and Oman [8], linearization of the Euler-Lagrange equations for the color channels u is performed using the fixed point iteration scheme, where the denominator is lagged by one iteration with respect to the numerator. The linearized functions are then optimized by the conjugate gradients method. The convergence of the fixed-point iteration scheme for L^1 fidelity term and MS regularizer for gray scale images has been proved by the authors [48].

Eqs. (15), (17) and (19) are linear with respect to v and are solved using the Minimal Residual algorithm. Note that with MS, MSTV and MSBEL regularization, there are four equations to solve. Studying the fidelity (11) and different regularization terms (5,6,7,9,10), it can be seen that they are strictly convex and lower bounded with respect to u^{σ} and v if the other variables are fixed. Therefore the minimization procedure alternates between u^{σ}, $\sigma \in \{r, g, b\}$ and v until a local minimizer is achieved.

Let $u_{i,j}^{\sigma}$ denote the discretized image function in channel σ. The forward and backward finite difference approximations of the derivatives $\partial u^{\sigma}(x,y)/\partial x$ and $\partial u^{\sigma}(x,y)/\partial y$ are respectively defined by

$$\Delta_{\pm}^{x} u_{i,j}^{\sigma} = \pm (u_{i\pm,j}^{\sigma} - u_{i,j}^{\sigma})$$

and

$$\Delta_{\pm}^{y} u_{i,j}^{\sigma} = \pm(u_{i,j\pm1}^{\sigma} - u_{i,j}^{\sigma}),$$

and the central finite differences approximation is

$$\Delta_{c}^{x} u_{i,j}^{\sigma} = (u_{i+1,j}^{\sigma} - u_{i-1,j}^{\sigma})/2$$

and

$$\Delta_{c}^{y} u_{i,j}^{\sigma} = (u_{i,j+1}^{\sigma} - u_{i,j-1}^{\sigma})/2.$$

The discretization of $||\nabla u||^2$ in Eqs. (15) (17) (19) was carried out using the central difference scheme

$$||\nabla u(x,y)||^2 = \sum_{\sigma\in\{r,g,b\}} (\Delta_{c}^{x} u_{i,j}^{\sigma})^2 + (\Delta_{c}^{y} u_{i,j}^{\sigma})^2.$$

Terms of the form $\nabla \cdot (C(x,y)\nabla u^{\sigma})$ and $\nabla^2 v$ were discretized using forward difference for the gradient and backward difference for the divergence

$$\nabla \cdot (C(x,y)\nabla u^{\sigma}) = \Delta_{-}^{x}\left(C(i,j)\Delta_{+}^{x} u_{i,j}^{\sigma}\right) + \Delta_{-}^{y}\left(C(i,j)\Delta_{+}^{y} u_{i,j}^{\sigma}\right).$$

The convolutions in Eqs. (12,13,14,16,18) were computed using the Fourier transform. As is well known, this necessitates very careful treatment of boundary conditions. In this case, the boundary conditions were implemented as follows. First, the image was extended by adding margins with half kernel width. These margins were obtained by replicating the one-pixel thick outer frame of the image. In addition, the multiplication of the FFT of two signals corresponds to their *circular* convolution. As a result, additional zero padding is necessary to eliminate aliasing. The algorithms were implemented in MATLAB® on a Pentium® 4 computer and run under 10 minutes for 256×256 color images. Computing time is dominated by FFT calculation, hence $O(N^2 \log N)$ effective dependence on $N \times N$ image size can be expected.

IV. Robust Statistics Interpretation

In this section, extending the results of [36], we provide a robust-statistics interpretation of the MS (7), MSTV (9) and MSBEL (10) regularizers. Consider the half-quadratic regularization [10], [49]. In this approach, the regularizer is a non-decreasing potential function $\xi(t)$, where in the context of image restoration $t = ||\nabla u||$. The key idea in the half-quadratic regularization is the representation of ξ as an infimum of a quadratic function E with an auxiliary variable b. Explicitly, if $\xi(\sqrt{t})$ is concave and non-decreasing, we can write

$$\xi(t) = \inf_{b} E(b,t)$$

such that

$$E = b\,t^2 + \Psi(b),$$

and $\Psi(b)$ is convex and decreasing. This representation is quadratic with respect to t when b is fixed, and therefore leads to easier optimization. In the case of edge-preserving image restoration, the auxiliary function b represents the edges. For example, the Geman and McClure (GM) [50] potential function corresponds to the half-quadratic form

$$\xi^{GM} = \inf_{b}\left(E^{GM}\right) = \frac{||\nabla u||^2}{1 + ||\nabla u||^2/\delta},$$

where

$$E^{GM} = b\,||\nabla u||^2 + \delta(\sqrt{b}-1)^2$$

and δ is a positive constant. Teboul *et al.* [51] noticed that in the presence of noise, image restoration benefits from well-behaved edges. Therefore an edge regularization term $\phi_b(b)$ was added to the smoothness term:

$$\mathcal{J} = \lambda_1 \int_\Omega \left[b||\nabla u||^2 + \Psi(b)\right] dA + \lambda_2 \int_\Omega \phi_b(b) dA.$$

In the case that $\Psi(b) = \delta(\sqrt{b}-1)^2$ and $\phi_b = |\nabla(\sqrt{b})|^2$,

$$\begin{aligned}\mathcal{J} =& \lambda_1 \int_\Omega \left[b||\nabla u||^2 + \delta(\sqrt{b}-1)^2\right] dA \\ &+ \lambda_2 \int_\Omega \left|\nabla(\sqrt{b})\right|^2 dA\ .\end{aligned} \tag{20}$$

Reordering the terms in the the MS regularizer in its Γ-convergence approximation (7) yields

$$\begin{aligned}\mathcal{J}_\varepsilon^{MS}(u,v) =\ & \beta \int_\Omega v^2 |\nabla u|^2\ dA + \ \alpha \int_\Omega \left(\frac{(v-1)^2}{4\varepsilon}\right)\ dA \\ &+ \alpha\varepsilon \int_\Omega |\nabla v|^2\ dA.\end{aligned} \tag{21}$$

Substituting $b = v^2$, $\lambda_1 = \beta$, $\delta = \alpha/4\varepsilon\beta$ and $\lambda_2 = \alpha\varepsilon$ yields equivalence between Eqs. (20) and (21). This regularizer is therefore the Geman-McClure function with an *additional spatial edge organization constraint*. Thus,

$$\mathcal{J}_\varepsilon^{MS} = \beta \int_\Omega E^{GM}\, dA + \alpha\varepsilon \int_\Omega |\nabla v|^2 dA \tag{22}$$

with $b = v^2$ and $\delta = \alpha/4\varepsilon\beta$. In the same manner, the functions that correspond to MSTV and MSBEL regularizers (9) (10) are

$$\begin{aligned}\mathcal{J}_\varepsilon^{MSTV} =& \beta \int_\Omega E^{MSTV}\, dA + \alpha\varepsilon \int |\nabla v|^2 dA; \\ \xi^{MSTV} =& \frac{\sqrt{\gamma + ||\nabla u||^2}}{1 + \sqrt{\gamma + ||\nabla u||^2/\delta}},\end{aligned} \tag{23}$$

and

$$\begin{aligned}\mathcal{J}_\varepsilon^{MSBEL} =& \beta \int_\Omega E^{MSBEL}\, dA + \alpha\varepsilon \int |\nabla v|^2 dA; \\ \xi^{MSBEL} =& \frac{||\nabla u||^2 + \gamma|u_x \times u_y|}{1 + (||\nabla u||^2 + \gamma|u_x \times u_y|)/\delta}.\end{aligned} \tag{24}$$

This observation explains the advantage of Mumford-Shah-like regularization. It applies a robust function for the detection of edges while demanding that these edges are smooth and continuous. This combination does not admit impulse noise as an edge. In addition, the L^1 fidelity term regards the impulse noise as an outlier and therefore reduces its influence. There is another mathematical facet to the advantage of the Mumford-Shah based stabilizer. Using the nonconvex Geman-Mcclure function as a regularizer, leads to the problem of a minimizer nonexistence [52]. By the additional spatial constraint, the existence of a minimizer is proved to be satisfied [52]. Thus, the Mumford-Shah based regularizer benefits a mathematical advantage in addition to the edge discrimination ability.

Fig. 1. Original 512×512 *Monarch* image

V. RESULTS

The methods we suggest in this work were tested on several images. We present some of the results here. In the first experiment we compare two different noise forms using two fidelity terms of Eqs. (3) and (4) with the Beltrami regularizer (6). As expected, fidelity term (3) with $\rho(s) = \sqrt{s^2 + \eta}$

$$\int_\Omega \sum_\sigma \sqrt{(h * u^\sigma - z^\sigma)^2 + \eta}\, dA \tag{25}$$

gives better results in the case of independent channels noise, while (4), specifically

$$\int_\Omega \sqrt{\sum_\sigma (h * u^\sigma - z^\sigma)^2 + \eta}\, dA \tag{26}$$

performs better in the presence of channel-dependent noise. The formation of the channel-independent salt-and-pepper noise was performed as follows [53]: the value of pixel (x, y) was replaced by 0 with probability $p/2$ and replaced by 1 with probability $p/2$ ($p \in [0, 1]$). In the case of dependent channels, pixel (x, y) was changed with probability p_1, and each channel of this pixel has been replaced by 0 or 1 with probability p_2. This means that in order to obtain the same number of damaged pixels using the two forms, the probabilities should satisfy $p = p_1 p_2$.

The 512×512 *Monarch* image is shown in Fig. 1 (fully) and in Fig. 2(a) (partially). The image was blurred by 7×7 out-of-focus kernel (Fig. 2(b)). The blurred image, corrupted by independent ($p = 0.3$) and dependent ($p_1 = 0.375$ and $p_2 = 0.8$) channel noise, is shown in Figs. 2(c) and 2(d) respectively.

Using Eqs. (25) and (26), the outcome of the restoration of Fig. 2(c) is shown in 2(e) and 2(g) respectively, while the restoration of 2(d) is presented in Figs. 2(f) and 2(h) respectively. In all cases the Beltrami regularizer (6) was used as smoothness term. Only part of the image is shown for better visibility of small details. As expected, fidelity term (25) visually gives better results in the case of independent channels, and (26) in the case of dependent channels. These observations are corroborated by the PSNR values given in Table I where

$$\mathrm{PSNR} = 10 \log_{10} \frac{3MN}{\sum_{i,j,\sigma} (I_{ij}^\sigma - u_{ij}^\sigma)^2}. \tag{27}$$

Here I^σ is the original $M \times N$ image at channel σ and u^σ is the corresponding recovered image.

In the next example we study a blurred image which was contaminated by different salt-and-pepper noise levels. The 256×256 *Lena* image which underwent blur with 7×7 out-of-focus kernel can be seen in Fig. 3.

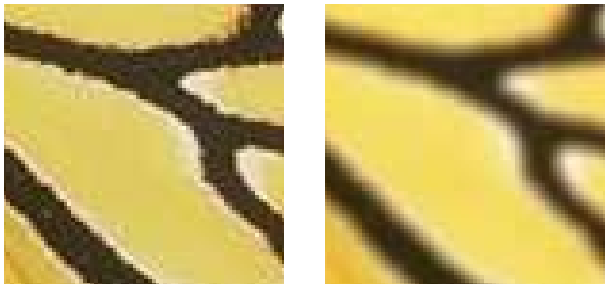

(a) - Original (b) - Blurred

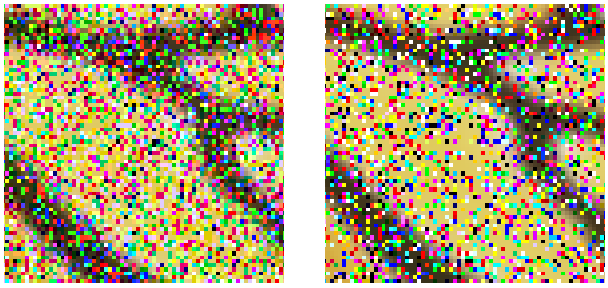

(c) - Independent Channels (d) - Dependent Channels

(e) - Recovery of (c) using Eq. (25)

(f) - Recovery of (d) using Eq. (25)

(g) - Recovery of (c) using Eq. (26)

(h) - Recovery of (d) using Eq. (26)

Fig. 2. Matching the fidelity term to the interchannel dependence characteristic of multichannel noise.

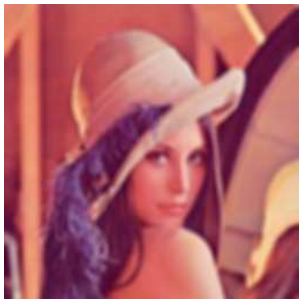

Fig. 3. *Lena* image blurred by 7×7 out-of-focus kernel

Fig. 4. Recovery of *Lena* image with 7×7 out-of-focus kernel with several salt-and-pepper noise levels

TABLE I

PSNR VALUES FOR FIGURE 2

	Independent Channels	Dependent Channels
Observed	9.62	9.60
Restored using Eq. (25)	23.15	22.87
Restored using Eq. (26)	22.64	23.31

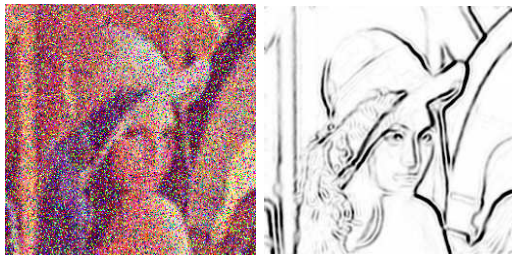

Fig. 5. Edge map v using the MS method recovery of blurred and noisy (0.3 density) *Lena* image

.

Restoration results of this image are shown in Fig. 4 where channel independent salt-and-pepper noise with $p = 0.01, 0.05, 0.1, 0.2, 0.3, 0.35$ was applied. Restoration was performed by the different regularizers and fidelity term (11). As can be seen in Fig. 4, there is no significant difference between the five methods in the case of low $(p = 0.01)$ noise density. When the noise level is increased, the methods based on the Mumford-Shah regularizer produce much better results than Beltrami or Total Variation regularizers. Note that in Fig. 4 for $p = 0.3$, color artifacts are nearly absent in the MS, MSTV and MSBEL regularizers, as opposed to green patches in the Beltrami and TV methods. The outcome of the MSTV regularization is more cartoon-like at all noise levels due to the robust constraint on the image gradients. These subjective observations are supported by the PSNR values shown in Table II. High PSNR values can be seen for Mumford-Shah, Mumford-Shah-TV and Mumford-Shah-Beltrami regularizers for all noise levels. The PSNR values do not however reflect the visually obvious differences between these three regularizers. The second (MSTV) produces much cleaner results, but suppresses most small details. In addition, note that using MS, MSTV, MSBEL regularizers provides the auxiliary function v. This function shown in Fig. 5 is well worth our attention since it provides an edge map of the color image.

The selected parameters are presented in Table IV. The parameter η was set to $\eta = 10^{-4}$ for all functionals, in all the results here and in the rest of the paper. The parameters were selected manually to provide the best PSNR results. It can be easily seen from the parameters table that the smoothness parameter β increases with noise level while the other parameters are approximately fixed. However, as long as the nature of the noise and the size of the image are kept constant, there is no need to adjust the parameters. Indeed, our experiments

TABLE II

PSNR VALUES FOR FIGURE 4

Noise Level	0.01	0.05	0.1	0.2	0.3	0.35
Observed	22.74	17.58	14.89	12.06	10.37	9.71
Beltrami	22.95	21.52	23.84	23.02	22.84	22.67
TV	22.94	21.62	23.89	23.52	23.45	23.60
MS	24,74	23.37	24.01	23.74	23.63	23.81
MSTV	23.85	23.89	23.78	23.67	24.02	24.02
MSBEL	23.79	23.42	24.09	24.06	23.80	24.01

TABLE III

PSNR VALUES FOR FIGURE 6

Kernel Length	4	6	8	10
Observed	19.18	18.81	18.52	18.23
Beltrami	22.23	20.79	22.52	21.98
TV	22.07	21.23	22.39	22.28
MS	22.45	22.49	22.68	22.71
MSTV	22.06	21.75	22.43	22.57
MSBEL	22.53	22.59	22.76	22.07

show that the proposed methods are not sensitive to small changes of the parameters.

In Fig. 6 we replaced the salt-and-pepper noise by a random channel independent impulse noise of 0.1 density. This means that 10% of the pixels were damaged and had a random value within the full dynamic range $[0, 1]$ of the channel. In this case we applied a motion-blur kernel oriented by 25° relative to the horizon with variable length of $4, 6, 8$ and 10. Parameters were set as in the previous experiment (see Table IV). The PSNR values of this experiment are presented in Table III. Visual observation of Fig. 6 shows as before the superiority of the MS, MSTV and MSBEL regularizers over Beltrami and Total Variation. Careful look at the PSNR table shows that for a given noise level, the Mumford-Shah-Beltrami regularizer performs better than the Mumford-Shah regularizer. This can be explained by the fact that the former has an additional constraint on the alignment of the gradients and therefore produces better recovery. Note that ringing artifacts that frequently plague deblurring algorithms, especially when some of the processing is performed in the frequency domain, are absent from our results.

In the final restoration example the image is degraded by a different process. In Fig. 7 we show restoration results for an image blurred by Gaussian kernel with $\sigma = 1.5$ corrupted by zero-mean Gaussian noise with $\sigma = 0.012$ and 1% $(p = 0.01)$ salt-and-pepper noise. The PSNR values in Table V show that in this case as well, the methods based on Mumford-Shah regularizer are superior to the Beltrami and Total Variation stabilizers, where Mumford-Shah-TV provides a slightly cleaner result but with loss of details. The parameters in this case

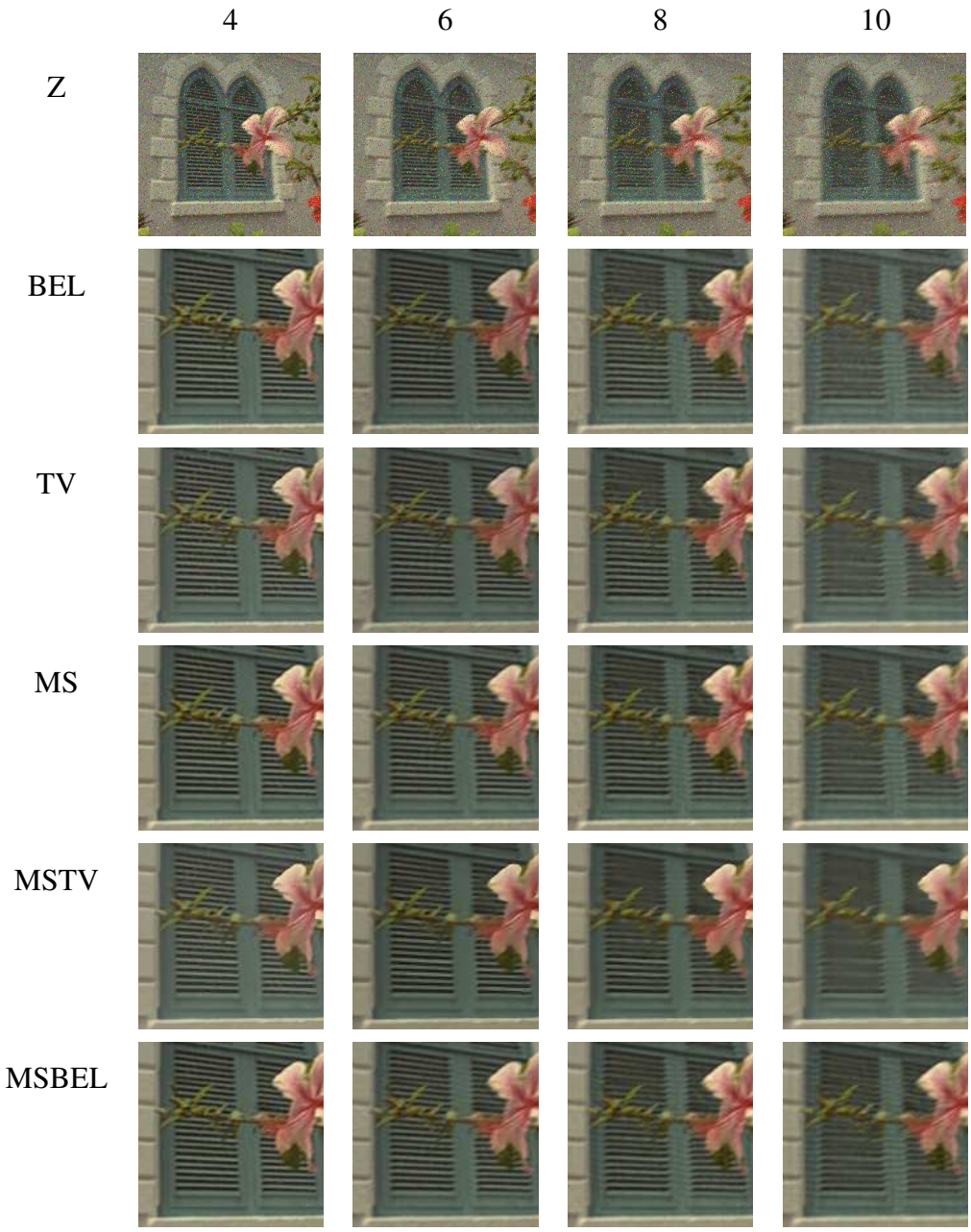

Fig. 6. Recovery of *Window* image with 0.1 impulse noise density and several motion blur levels

were set as in the first experiment (Table IV $p = 0.01$).

VI. Discussion

In this research, we addressed the problem of color image deblurring in the presence of impulsive noise. It is well known that channel-by-channel restoration of color images is inefficient, and that some coupling between the channels is required. Adopting the variational framework, the cost functionals that we considered consist of a modified L^1 fidelity norm with channel coupling, and one of several multichannel regularization terms.

We have presented five types of regularization terms: a channel-coupled version of the Total Variation

TABLE IV

PARAMETERS SELECTION FOR ALL EXPERIMENTS

Noise Level	0.01	0.05	0.1	0.2	0.3	0.35
β^{BEL}	10^{-3}	10^{-3}	0.8	1.0	1.2	1.25
γ^{BEL}	0.1	0.1	0.1	0.1	0.1	0.1
β^{TV}	10^{-4}	10^{-3}	0.1	0.15	0.2	0.25
$\beta^{MS,MSBEL}$	0.05	0.1	0.7	1.6	2.2	2.25
β^{MSTV}	0.05	0.1	0.5	0.8	1.1	1.5
$\alpha^{MS,MSBEL}$	0.1	0.1	0.5	0.5	0.5	0.5
α^{MSTV}	0.1	0.1	0.1	0.1	0.5	0.5
$\varepsilon^{MS,MSTV,MSBEL}$	0.1	0.1	0.1	0.1	0.1	0.1
γ^{MSBEL}	1	1	1	1	1	1
μ^{MSTV}	$2 \cdot 10^{-3}$	$2 \cdot 10^{-3}$	$2 \cdot 10^{-3}$	$2 \cdot 10^{-3}$	$2 \cdot 10^{-3}$	$2 \cdot 10^{-3}$

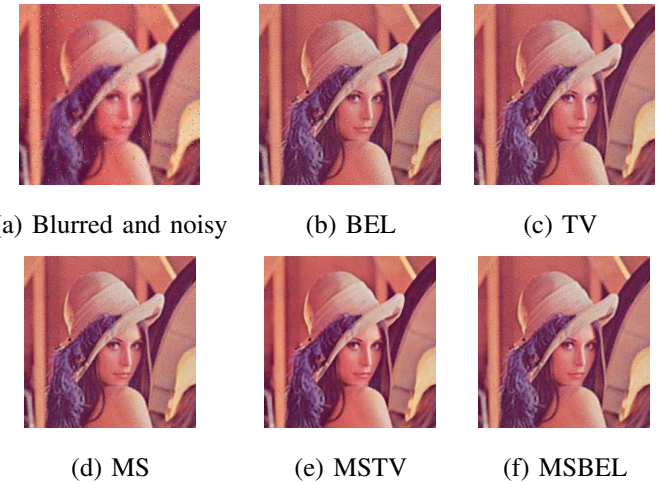

(a) Blurred and noisy (b) BEL (c) TV

(d) MS (e) MSTV (f) MSBEL

Fig. 7. Recovery of the *Lena* image blurred by 7×7 out-of-focus kernel contaminated by a mixture of Gaussian and salt-and-pepper noise

TABLE V

PSNR VALUES FOR FIGURE 7

Observed	22.67
Beltrami	26.21
TV	26.43
MS	27.20
MSTV	29.16
MSBEL	27.29

norm (TV), Beltrami (BEL) flow, multichannel extensions of elements from the Mumford-Shah segmentation functional (MS), a Total Variation version of the above MS regularizer (MSTV) and combination of Beltrami and MS regularizer (MSBEL).

From theoretical and experimental points of view, the three Mumford-Shah type regularization techniques (MS, MSTV, MSBEL) are superior with respect to the Total Variation and Beltrami flow stabilizers because they reflect the underlying piecewise-smooth image model together with the channel coupling property, and hence result in cleaner restoration and also yields an image edge map. The Total Variation Mumford-Shah regularizer (MSTV) is more robust than the MS stabilizer to image gradients, and therefore drives the recovered image towards the piecewise constant limit. In the case of high noise density, the cartoon-like restored image is much cleaner than the recovered image using the other methods.

With the Mumford-Shah based methods in their Γ-convergence approximation (MS, MSTV, MSBEL), edges are detected concurrently with the deblurring process and the bias towards continuous edges ($|\nabla v|^2$) in Eqs. (7) (9) (10) is inherently embedded in the cost functional. Edge continuity is the ideal discriminant between outliers, i.e., isolated edge-like points, and genuine image edges. Our experimental results support the theoretical observations.

As shown in the previous section, the sensitivity to parameter values is moderate. Different images with different blur kernels and noise types (salt-and-pepper, impulse) shared the same parameter set for a given noise density.

REFERENCES

[1] G. Demoment, "Image reconstruction and restoration: Overview of common estimation structures and problems," *IEEE Trans. Acoust. Speech, Signal Processing*, vol. 37, no. 12, pp. 2024–2036, 1989.

[2] J. Biemond, R. Lagendijk, and R. Mersereau, "Iterative methods for image deblurring," *Proc. IEEE*, vol. 78, no. 5, pp. 856–883, 1990.

[3] M. Banham and A. Katsaggelos, "Digital image restoration," *IEEE Signal Processing Mag.*, vol. 14, pp. 24–41, 1997.

[4] R. Puetter, T. Gosnell, and A. Yahil, "Digital image reconstruction: Deblurring and denoising," *Annu. Rev. Astron. Astrophys.*, vol. 43, pp. 139–194, 2005.

[5] L. Rudin, S. Osher, and E. Fatemi, "Non linear total variatrion based noise removal algorithms," *Physica D*, vol. 60, pp. 259–268, 1992.

[6] S. Geman and D. Geman, "Stochastic relaxation, Gibbs distribution, and the Bayesian restoration of images," *IEEE Trans. Pattern Anal. Mach. Intell.*, vol. 6, pp. 721–741, 1984.

[7] C. Vogel and M. Oman, "Iterative methods for total variation denoising," *SIAM Journal on Scientific Computing*, vol. 17, no. 1, pp. 227–238, January 1996.

[8] ——, "Fast, robust total variation-based reconstruction of noisy, blurred images," *IEEE Trans. Image Processing*, vol. 7, pp. 813–824, 1998.

[9] D. Geman and G. Reynolds, "Constrained restoration and recovery of discontinuities," *IEEE Trans. Pattern Analysis and Machine Intelligence*, vol. 14, no. 3, pp. 367–383, March 1992.

[10] D. Geman and C. Yang, "Nonlinear image recovery with half-quadratic regularization," *IEEE Trans. Image Processing*, vol. 4, pp. 932–946, July 1995.

[11] R. Neelmani, H. Choi, and R. Baraniuk, "Forward: Fourier-wavelet regularized deconvolution for ill-conditioned systems," *IEEE Trans.Image Processing*, vol. 52, no. 2, pp. 418–433, February 2004.

[12] M. Nikolova, J. Idier, and A. Mohammad-Djafari, "Inversion of large-support ill-posed linear operators using a piecewise gaussian MRF," *IEEE Trans. Image Processing*, vol. 8, no. 4, April 1998.

[13] P. Combettes and J. Luo, "An adaptive level set method for nondifferentiable constrained image recovery," *IEEE Trans. Image Processing*, vol. 11, pp. 1295–1304, November 2002.

[14] M. Nikolova, "Minimizers of cost-functions involving nonsmooth data-fidelit y terms: Application to the processing of outliers," *SIAM Journal on Numerical Analysis*, vol. 40, pp. 965–994, 2002.

[15] ——, "A variational approach to remove outliers and impulse noise," *Journal of Mathematical Imaging and Vision*, vol. 20, pp. 99–120, 2004.

[16] R. Chan, C. Ho, and M. Nikolova, "Salt-and-pepper noise removal by median-type noise detectors and edge-preserving regularization," *IEEE Trans. Image Processing*, vol. 14, no. 10, pp. 1479–1485, 2005.

[17] N. Galatsanos, M. Wernick, A. Katsaggelos, and R. Molina, "Multichannel image recovery," in *Handbook of Image and Video Processing*, 2nd ed., A. C. Bovik, Ed. Academic Press, 2005, pp. 203–218.

[18] A. Brook, R. Kimmel, and N. Sochen, "Variational restoration and edge detection for color images," *J. Math. Imaging Vision*, vol. 18, pp. 247–268, 2003.

[19] D. Tschumperlé, "PDE's based regularization of multivalued images and applications," Ph.D. dissertation, University of Nice–Sophia Antipolis, 2002.

[20] S. Di Zenzo, "A note on the gradient of a multi-image," *Computer Vision, Graphics, and Image Processing*, vol. 33, no. 1, pp. 116–125, 1986.

[21] A. Cumani, "Edge detection in multispectral images," *CVGIP: Graphical Models and Image Processing*, vol. 53, no. 1, pp. 40–51, 1991.

[22] G. Sapiro and D. Ringach, "Anisotropic diffusion of multivalued images with application to color filtering," *IEEE Trans. Image Processing*, vol. 5, no. 11, pp. 1582–1586, Oct. 1996.

[23] P. Blomgren, "Total variation methods for restoration of vector valued images," Ph.D. dissertation, University of California, Los-Angeles, 1998.

[24] N. Sochen, R. Kimmel, and R. Malladi, "A general framework for low level vision," *IEEE Trans. Image Processing*, vol. 7, pp. 310–318, 1998.

[25] D. Barash, "One-step deblurring and denoising color images using partial differential equations," in *First SIAM Conference on Imaging Science*, Boston, MA, 2002.

[26] M. Welk, D. Theis, T. Brox, and J. Weickert, "PDE-based deconvolution with forward-backward diffusivities and diffusion tensors," in *Proc. of 5th International Conference on Scale Space and PDE Methods in Computer Vision*, ser. LNCS, vol. 3439, 2005, pp. 585–597.

[27] P. Perona and J. Malik, "Scale-space and edge detection using anisotropic diffusion," *IEEE Trans. Pattern Analysis and Machine Intelligence*, vol. 12, pp. 629–639, 1990.

[28] R. Molina, J. Mateos, A. Katsaggelos, and M. Vega, "Bayesian multichannel image restoration using compound Gauss-Markov random fields," *IEEE Trans. Image Processing*, vol. 12, pp. 1642–1654, 2003.

[29] J. Astola, P. Haavisto, and Y. Neuvo, "Vector median filters," *Proc. IEEE*, vol. 78, no. 4, pp. 678–689, 1990.

[30] P. Trahanias and A. Venetsanopoulos, "Vector directional filters—a new class of multichannel image processing filters," *IEEE Trans. Image Processing*, vol. 2, no. 4, pp. 528–534, 1993.

[31] P. Trahanias, D. Karakos, and A. Venetsanopoulos, "Directional processing of color images: Theory and experimental results," *IEEE Trans. Image Processing*, vol. 5, no. 6, pp. 868–880, 1996.

[32] H. Hwang and R. Haddad, "Adaptive median filters: New algorithms and results," *IEEE Trans. Image Processing*, vol. 4, no. 4, pp. 499–502, 1995.

[33] F. Cheikh, R. Hamila, M. Gabbouj, and J. Astola, "Impulse noise removal in highly corrupted color images," in *Proc. of International Conference on Image Processing*, vol. 1, 1996, pp. 997 – 1000.

[34] R. Lukac, B. Smolka, K. Martin, K. Plataniotis, and A. Venetsanopoulos, "Vector filtering for color imaging," *IEEE Signal Processing Mag.*, vol. 22, no. 1, pp. 74–86, 2005.

[35] L. Bar, N. Sochen, and N. Kiryati, "Image deblurring in the presence of salt-and-pepper noise," in *Proc. of 5th International Conference on Scale Space and PDE Methods in Computer Vision*, ser. LNCS, vol. 3459, 2005, pp. 107–118.

[36] ——, "Image deblurring in the presence of impulsive noise," *International Journal of Computer Vision*, vol. 70, pp. 279–298, 2006.

[37] P. Huber, *Robust Statistics*. John Wiley and Sons, New York, 1981.

[38] M. Black and A. Rangarajan, "On the unification of line processes, outlier rejection, and robust statistics with applications in early vision," *International Journal of Computer Vision*, vol. 19, pp. 57–92, 1996.

[39] P. Blomgren and T. Chan, "Color TV: Total variation methods for restoration of vector-valued images," *IEEE Trans. Image Processing*, vol. 7, pp. 304–309, 1998.

[40] R. Kimmel, R. Malladi, and N. Sochen, "Images as embedded maps and minimal surfaces: Movies, color, texture, and volumetric medical images," *International Journal of Computer Vision*, vol. 39, pp. 111–129, 2000.

[41] D. Mumford and J. Shah, "Optimal approximations by piecewise smooth functions and associated variational problems," *Comm. Pure Appl. Math.*, vol. 42, pp. 577–685, 1989.

[42] L. Bar, N. Sochen, and N. Kiryati, "Variational pairing of image segmentation and blind restoration," in *Proc. of 8th European Conference on Computer Vision*, ser. LNCS, vol. 3022, 2004, pp. 166–177.

[43] L. Ambrosio and V. Tortorelli, "Approximation of functionals depending on jumps by elliptic functionals via Γ-convergence," *Comm. Pure Appl. Math.*, vol. 43, no. 8, pp. 999–1036, 1990.

[44] J. Shah, "A common framework for curve evolution, segmentation and anisotropic diffusion," in *Proc. of IEEE Conference on Computer Vision and Pattern Recognition*, 1996, pp. 136–142.

[45] R. Alicandro, A. Braides, and J. Shah, "Free-discontinuity problems via functionals involving the L^1-norm of the gradient and their approximation," *Interfaces and Free Boundaries*, vol. 1, pp. 17–37, 1999.

[46] D. Strong and T. Chan, "Edge-preserving and scale dependent properties of total variation regularization," UCLA Math department, CAM Report 00–38, 2000.

[47] R. Kaftori, N. Sochen, and Y. Zeevi, "Color image denoising and blind deconvolution using the Beltrami operator," in *Proceedings of the 3rd International Symposium on Image and Signal Processing and Analysis*, vol. 1, 2003, pp. 1–4.

[48] L. Bar, "Variational image restoration with segmentation-based regularization," Ph.D. dissertation, University of Tel-Aviv, 2006.

[49] P. Charbonnier, L. Blanc-Féraud, G. Aubert, and M. Barlaud, "Deterministic edge-preserving regularization in computed imaging," *IEEE Trans. Image Processing*, vol. 6, pp. 298–311, 1997.

[50] S. Geman and D. McClure, "Bayesian image analysis: An application to single photon emission tomography," *Proc. Amer. Statist. Assoc. Statistical Computing Section*, pp. 12–18, 1985.

[51] S. Teboul, L. Blanc-Féraud, G. Aubert, and M. Barlaud, "Variational approach for edge-preserving regularization using coupled PDE's," *IEEE Trans. Image Processing*, vol. 7, pp. 387–397, 1998.

[52] M. Chipot, R. March, M. Rosati, and G. Caffarell, "Analysis of a nonconvex problem related to signal selective smoothing," *Mathematical Models and Methods in Applied Science*, vol. 7, pp. 313–328, 1997.

[53] C. Boncelet, "Image noise models," in *Handbook of Image and Video Processing*, A. C. Bovik, Ed. Academic Press, 2000, pp. 325–335.